PNAS RESEARCH ARTICLE | DEVELOPMENTAL BIOLOGY OPEN ACCESS

Mafba and Mafbb regulate microglial colonization of zebrafish brain via controlling chemotaxis receptor expression

Liang Lou[a,1], Tao Yu[b,c,1], Yimei Dai[d], Shizheng Zhao[a], Shachuan Feng[a], Jin Xu[d], and Zilong Wen[a,b,c,2]

Edited by Marco Colonna, Washington University in St. Louis School of Medicine, St. Louis, MO; received February 22, 2022; accepted August 4, 2022

Microglia are the central nervous system (CNS)–resident macrophages involved in neural inflammation, neurogenesis, and neural activity regulation. Previous studies have shown that naturally occurring neuronal apoptosis plays a critical role in regulating microglial colonization of the brain in zebrafish. However, the molecular signaling cascades underlying neuronal apoptosis-mediated microglial colonization and the regulation of these cascades remain undefined. Here, we show that basic leucine zipper (b-Zip) transcription factors, Mafba and Mafbb, two zebrafish orthologs of mammalian MAFB, are key regulators in neuronal apoptosis-mediated microglial colonization of the brain in zebrafish. We document that the loss of Mafba and Mafbb function perturbs microglial colonization of the brain. We further demonstrate that Mafba and Mafbb act cell-autonomously and cooperatively to orchestrate microglial colonization, at least in part, by regulating the expression of G protein–coupled receptor 34a (Gpr34a), which directs peripheral macrophage recruitment into the brain through sensing the lysophosphatidylserine (lysoPS) released by the apoptotic neurons. Our study reveals that Mafba and Mafbb regulate neuronal apoptosis-mediated microglial colonization of the brain in zebrafish via the lysoPS-Gpr34a pathway.

microglia | colonization | Mafb | lysoPS | Gpr34a

Microglia are the central nervous system (CNS)–resident macrophages, and they play versatile roles in the CNS (1). As the key immune cells in the CNS, microglia are constantly engaged in the removal of toxic protein plaques, cell debris, pathogens, and damaged/dying cells to maintain the homeostasis of the CNS (2). In addition to functioning as immune cells, emerging evidences have indicated that microglia are also actively involved in regulating neural development and neural functions, including synaptic pruning, suppressing neuronal activity, and modulating synaptic plasticity (3). Moreover, microglial dysfunction has been found to associate with the onset and progression of various neurodegenerative disorders, such as Alzheimer's disease, Parkinson disease, and multiple sclerosis (4, 5). Thus, elucidating the principle governing microglial formation and functions will enhance our understanding of the development of these neurodegenerative diseases and may provide new therapeutic approaches for the treatment of these disorders.

Unlike neuroectoderm origin of neurons, astrocytes, and oligodendrocytes, several fate-mapping studies in mice have revealed that microglia arise from erythromyeloid progenitors (EMPs) that are born in the extraembryonic yolk sac (6–8). Shortly after emergence from the yolk sac, these EMPs start to travel from the yolk sac to colonize the brain rudiment before E9.5 (8, 9). Although subsequent positioning of microglia to the subventricular zone and the barrel centers has been suggested to be mediated by two chemokines, CXCL12 and CX3CL1, respectively (10, 11), the mechanisms underlying the homing of peripheral macrophages from peripheral tissues to the CNS and their subsequent distribution in different CNS compartments in mammals remain largely unknown. Recently, by combining genetic manipulation and time-lapse imaging, several studies in zebrafish have elegantly shown that Il34-Csf1ra signaling and neuronal apoptosis act synergistically to promote peripheral macrophages to colonize different CNS compartments (12–14). The neuron-derived chemokine Il34 serves as a long-range signal to recruit peripheral macrophages from the rostral blood island (RBI), a hematopoietic tissue equivalent to the mouse yolk sac for myelopoiesis (15, 16), to migrate to the head region and subsequently colonize the brain and retina (12). In parallel, the naturally occurring neuronal apoptosis provides short-range signals such as lysophosphatidylcholine (LPC) and ATP to attract neighboring microglial precursors to colonize the optic tectum (13, 14). Although these studies highlight the significance of neuronal apoptosis in microglial colonization, the molecular cues released by apoptotic neurons and the receptors in microglia, as well as their upstream regulators, remain incompletely defined.

Significance

Microglia are a subpopulation of macrophages residing in the central nervous system (CNS). Because microglial precursors/peripheral macrophages are born in peripheral hematopoietic tissues, the establishment of a microglia pool in the CNS involves two processes: colonization, the homing of macrophages from peripheral tissues to the CNS, and maturation, the differentiation of brain-colonizing macrophages into microglia. This study aims to investigate the molecular mechanisms underlying microglial colonization during early development. Utilizing a zebrafish model system, we show that Mafba and Mafbb, two zebrafish orthologs of mammalian MAFB essential for macrophage differentiation and phagocytosis, regulate microglial colonization of the brain via modulating the lysoPS-Gpr34a signaling pathway during early embryogenesis. Our findings reveal a previously unappreciated genetic mechanism involved in microglial colonization of the brain.

Author contributions: L.L., T.Y., J.X., and Z.W. designed research; L.L., T.Y., and Y.D. performed research; L.L., T.Y., Y.D., S.Z., S.F., J.X., and Z.W. analyzed data; and L.L., T.Y., and Z.W. wrote the paper.

The authors declare no competing interest.

This article is a PNAS Direct Submission.

[1]L.L. and T.Y. contributed equally to this work.

[2]To whom correspondence may be addressed. Email: zilong@ust.hk.

This article contains supporting information online at http://www.pnas.org/lookup/suppl/doi:10.1073/pnas.2203273119/-/DCSupplemental.

Published September 19, 2022.

MAFB is a member of large MAF transcription factor family, which contains a basic leucine zipper domain (b-Zip) for dimerization and binding to MAF recognition elements (MARE) as well as a transactivation domain for regulation of target gene transcription (17). MafB is expressed in a variety of cell types, such as pancreatic α cells, renal podocytes, hair follicles, and hematopoietic cells (17). In hematopoietic systems, MafB is highly enriched in monocytes and macrophages (17) and has been shown to be involved in the regulation of macrophage terminal differentiation (18–20), osteoclastogenesis (21, 22), macrophage phagocytosis (23, 24), as well as foam cells apoptosis (25). In addition, a recent study of microglia transcriptomic analysis reveals that MafB is expressed predominantly in adult microglia and plays an essential role in suppressing antiviral response pathways in adulthood (26). Intriguingly, in their RNA sequencing (RNA-seq) data, MafB expression is also detected in microglia during early development of mouse embryos (26), indicating a potential role of MafB in microglia development. However, perhaps due to either embryonic lethality of MafB-null mice (27) or technical challenging in directly visualizing microglia during early mouse development, the role of MafB in the establishment of a microglia pool during early development remains unexplored.

In this study, we employed genetic manipulation and in vivo time-lapse imaging to demonstrate that microglia colonization of the developing zebrafish brain is governed by Mafba and Mafbb, two zebrafish orthologs of mammalian MAFB, through regulating the expression of the G protein coupled receptor 34a (Gpr34a), which in turn is capable of sensing lysophosphatidylserine (lysoPS) released from apoptotic neurons.

Results

Mafba and Mafbb Regulate Microglia Formation Cell-Autonomously during Early Zebrafish Development. To probe the function of MafB in microglia development during early embryogenesis, we focused on transcription factors Mafba and Mafbb, the two zebrafish orthologs of mammalian MAFB, which share 50–70% similarities in protein sequences (*SI Appendix*, Fig. S1*A*) and are also highly expressed in microglia during early development (*SI Appendix*, Fig. S1*B*). We utilized CRISPR-Cas9 system to generate a null allele *mafbb*$^{\Delta 504}$, which harbors 505-bp deletion and 7-bp insertion and additional 6-bp deletion in the coding region of *mafbb* gene, leading to the production of a truncated protein lacking the transactivation domain (*SI Appendix*, Fig. S1 *C* and *D*). We crossed *mafbb*$^{\Delta 504}$ with *mafba*^{uq4bh} (referred to as *mafbb* mutant and *mafba* mutant hereafter, respectively) (28) to create *mafba* and *mafbb* double mutants (referred to as DMut hereafter) and asked whether inactivation of Mafba and Mafbb alone or both together would interfere with the development of microglia. Neutral red (a dye that stains the lysosome of microglia) (29) staining revealed that, while the numbers of neutral red positive (NR$^+$) microglia in *mafba* and *mafbb* single mutants were either comparable to that in siblings (*sib*) (refer to *mafbb* heterozygotes or *mafba/b* double heterozygotes) or only marginally reduced, the NR$^+$ microglia in DMut were significantly decreased (*SI Appendix*, Fig. S1 *E* and *F*).

To confirm the decrease of NR signals in DMut was due to the reduction of microglia number, not due to the lysosomal defect of microglia, we crossed DMut with *Tg(mpeg1:loxp-DsRedx-loxp-eGFP)* line (referred to as *Tg(mpeg1:DsRedx)* hereafter) (13), in which microglia and peripheral macrophages are marked by DsRedx. Consistent with the NR staining, we found that DsRedx$^+$ microglia were drastically reduced in the brain of DMut compared to those in siblings, *mafba* single mutants, and *mafbb* single mutants (Fig. 1 *A* and *B*). The reduction of microglia in DMut was evident from 3 d post fertilization (dpf) to 6 dpf, suggesting that this phenotype is not caused by the developmental delay of the mutant embryos (*SI Appendix*, Fig. S1*G*).

Because *mafba* is also expressed in nonmicroglial cells in the brain (*SI Appendix*, Fig. S1*B*), we were therefore keen to know whether the microglial phenotype in DMut was caused by a cell-autonomous or a non-cell-autonomous effect. To address this issue, we generated two transgenic lines, *Tg(mfap4:mafba-P2a-DsRedx)* and *Tg(mfap4:mafbb-P2a-DsRedx)*, in which *mafba* and *mafbb* was overexpressed in microglia and macrophages under the control of the macrophage-specific *mfap4* promoter (30), and asked if the restoration of either *mafba* or *mafbb* expression in microglia was able to rescue the microglial phenotype in DMut. Results showed that the reconstitution of either *mafba* or *mafbb* was sufficient to rescue microglia number in DMut (Fig. 1 *C*–*E*). Taken together, these data indicate that Mafba and Mafbb act cooperatively to regulate the development of microglia in a cell-autonomous manner.

Deficiency of Mafba and Mafbb Impairs Microglial Colonization of the Optic Tectum. To have a better understanding of the cellular basis underlying the reduction of microglia in DMut, we examined the formation of microglial precursors/peripheral macrophages from 2.5 dpf to 3 dpf. Results showed that the numbers of peripheral macrophages in single mutants and DMut were either comparable (*mafbb*) to that in control siblings or only marginally decreased (*mafba* and DMut) (Fig. 2*A* and *SI Appendix*, Fig. S2*A*). The marginal decrease of peripheral macrophages could not fully explain the dramatic reduction of microglia in DMut (Fig. 1 *A* and *B*), suggesting that other cellular defect, such as the impairment of microglia brain colonization, likely contribute to the microglial phenotype in DMut. To support this hypothesis, we outcrossed DMut fish with *Tg(-2.8elavl3:eGFP;mpeg1:DsRedx)* reporter line, in which the neurons and microglia/macrophages were labeled by GFP and DsRedx, respectively (13), and performed time-lapse imaging to monitor the mobilization of peripheral macrophages and their ability to colonize the brain. As we anticipated, while abundant DsRed$^+$ microglial precursors (around 14–15 cells) were found to colonize the brain in siblings and *mafba* single mutants from the period of 2.5 dpf to 3 dpf, very few colonization events (around 2 on average) were observed in DMut (Fig. 2 *B* and *C*). This colonization defect in DMut was due to neither the impairment of general migratory ability of peripheral macrophages, as the basal motility of these cells was comparable between DMut and siblings (*SI Appendix*, Fig. S2*B*), nor the deterioration of directional migration in response to stimuli, as the peripheral macrophages in DMut responded normally to tail fin injury and *E. coli* inoculation (Fig. 2 *D* and *E* and *SI Appendix*, Fig. S2 *C* and *D*). Taken together, these data demonstrate that Mafba and Mafbb play a critical role in regulating peripheral macrophage brain colonization but are dispensable for injury- and pathogen-induced migration of macrophages.

Neuronal Apoptosis-Mediated Microglial Colonization Is Perturbed in DMut. Previous studies have revealed two independent signaling pathways, Il34-Csf1ra pathway and neuronal apoptosis signaling, which act cooperatively to orchestrate microglial colonization of different compartments of zebrafish brain (12, 13). To uncover which of these signaling pathways was perturbed in DMut, we first examined the colonization pattern of microglia

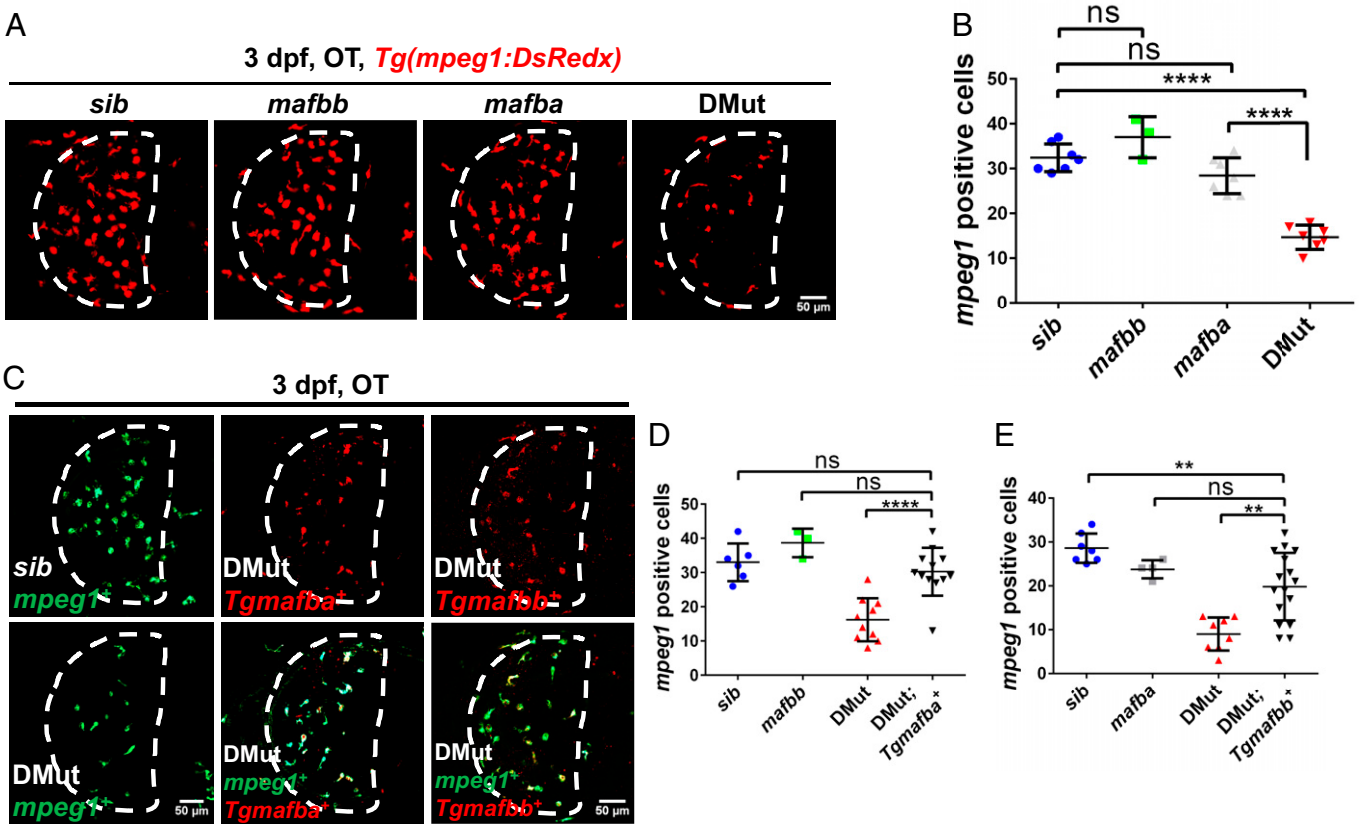

Fig. 1. Mafba and Mafbb regulate microglia development cell-autonomously during zebrafish early development. (*A*) Representative images of microglia in the optic tectum (OT) in 3 dpf siblings, *mafba* mutants, *mafbb* mutants, and DMut embryos in *Tg(mpeg1:DsRedx)* transgenic background. Microglia are labeled in DsRed. Dashed lines indicate the optic tectum region. (*B*) Quantification of microglia number in the OT in 3 dpf siblings ($n = 7$), *mafba* mutants ($n = 7$), *mafbb* mutants ($n = 3$), and DMut ($n = 7$) (mean ± SD; Student's *t* test; nonsignificant [ns] $P > 0.05$, ****$P < 0.0001$). (*C*) Representative images of microglia in the OT in 3 dpf siblings, DMut embryos, DMut;*Tg(mfap4:mafba-P2a-DsRedx)* transgenic embryos, and DMut;*Tg(mfap4:mafbb-P2a-DsRedx)* transgenic embryos. Microglia are labeled in green color in *Tg(mpeg1:eGFP)* transgenic background. The overexpression of *mafba* and *mafbb* is indicated by red color in *Tg(mfap4:mafba-P2a-DsRedx)* and *Tg(mfap4:mafbb-P2a-DsRedx)* transgenic lines, respectively. Dashed lines indicate OT region. (*D* and *E*) Quantification of microglia in the OT in 3 dpf siblings ($n = 6$ or 7), *mafba* mutants ($n = 4$), *mafbb* mutants ($n = 3$), DMut ($n = 10$ or 8), DMut;*Tg(mfap4:mafba-P2a-DsRedx)* transgenic embryos ($n = 12$), and DMut;*Tg(mfap4:mafbb-P2a-DsRedx)* transgenic embryos ($n = 16$) (mean ± SD; Student's *t* test; nonsignificant [ns] $P > 0.05$, **$P < 0.01$, ****$P < 0.0001$).

in different regions of DMut brain and compared it with that of *il34*-deficient mutants and *Tg(Xla.Tubb:bcl-2)* fish, in which the Il34-Csf1ra signaling and neuronal apoptosis pathway was largely abolished, respectively (12, 13). We found that the reduction of microglia in DMut was most prominent in the optic tectum (74% reduction compared to siblings) (*SI Appendix*, Fig. S3), a phenotype similar to that of *Tg(Xla.Tubb:bcl-2)* line (12), suggesting that the response of peripheral macrophages to neuron apoptotic signals is likely disrupted in DMut. To further confirm this was indeed the case, we outcrossed the mutant fish with *Tg(neurod1:Gal4FF;UAS:Eco.NfsB-mCherry)* line (31, 32) and tested whether the peripheral macrophages in DMut responded normally to metronidazole (MTZ)-induced neuronal apoptosis in the spinal cord (33). We found that, while abundant macrophages were found to accumulate around the spinal cord region in control siblings, *mafba* and *mafbb* single mutants upon MTZ treatment, no significant increase of macrophage accumulation was observed around the spinal cord region in DMut (Fig. 3 *A* and *B* and *SI Appendix*, Fig. S4 *A* and *B*). Time-lapse imaging further revealed that the percentage of macrophages migrating to the spinal cord region in DMut was significantly lower than that in siblings after MTZ treatment (Fig. 3 *C* and *D*). In addition, we tracked the migration paths of the macrophages that responded to MTZ-induced neuronal apoptosis and measured three parameters: the distance of each cell from the spinal cord region at T0, the total distance traveled by each cell, and the mean velocity of each cell. Results showed that the total average distance traveled by each macrophage and the average distance of each macrophage from the spinal cord at T0 were similar between siblings and DMut after MTZ treatment (*SI Appendix*, Fig. S4 *C* and *D*), while the mean velocity of each macrophage was marginally, but not significantly, decreased in DMut compared to siblings (*SI Appendix*, Fig. S4*E*). This indicates that, while a smaller percentage of macrophages respond to MTZ-induced neuronal apoptosis in DMut, the directional migration and the basal motility of the responding macrophages remains largely unaffected. Taken together, these results demonstrate that the response of peripheral macrophages to neuron apoptotic signals is severely impaired in DMut. In contrast, the Il34-Csf1ra signaling pathway appeared to be unaffected in DMut, as no alteration of *csf1ra* expression was observed in the microglia between DMut and control siblings (*SI Appendix*, Fig. S5). Collectively, from these data, we conclude that the reduction of microglia in DMut is largely attributed to the unresponsiveness of peripheral macrophages to the signals released from the apoptotic neurons.

Mafba and Mafbb Regulate Microglial Colonization through Controlling Chemotaxis Receptor Expression. To understand the molecular basis underlying the unresponsiveness of macrophages to the neuron apoptotic signals in DMut, we isolated microglia from siblings, *mafba* and *mafbb* single mutants, and DMut and performed whole-transcriptome analysis (Fig. 4*A*).

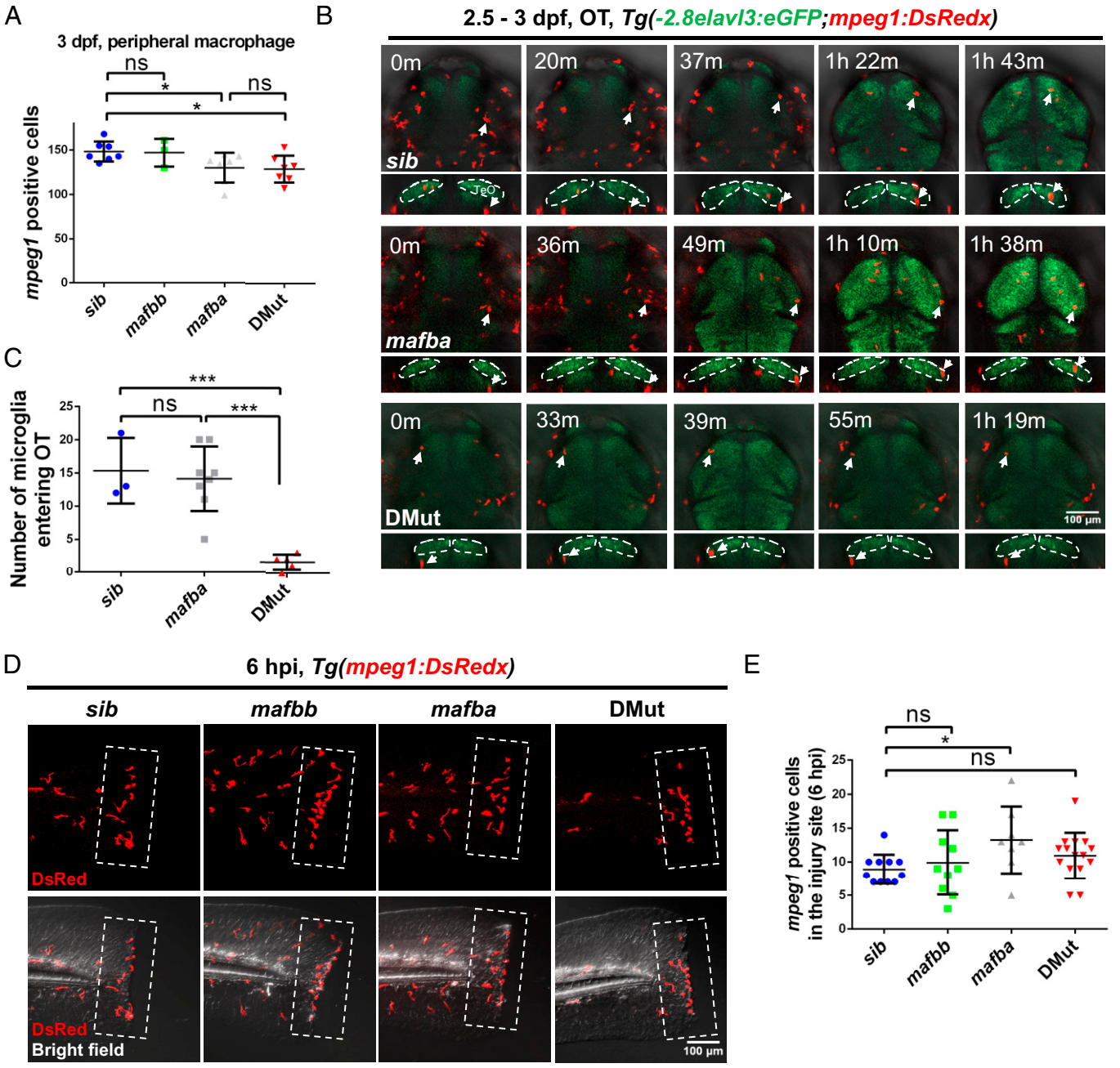

Fig. 2. Microglia colonization of the optic tectum is defective in DMut. (*A*) Quantification of peripheral macrophages in 3 dpf siblings ($n = 7$), *mafba* mutants ($n = 7$), *mafbb* mutants ($n = 3$), and DMut ($n = 7$) in *Tg(mpeg1:DsRedx)* background (mean ± SD; Student's *t* test; nonsignificant [ns] $P > 0.05$, $^*P < 0.05$). (*B*) Coronal and transverse views of time-lapse imaging pictures of the midbrain of siblings, *mafba* mutants, and DMut in *Tg(-2.8elavl3:eGFP;mpeg1:DsRedx)* transgenic background where microglia are labeled in red and neurons are marked in green. Dashed lines indicate the optic tectum (OT) region. White arrows indicate microglia that have entered the OT. (*C*) Quantification of microglia number entering the OT in siblings ($n = 3$), *mafba* mutants ($n = 8$), and DMut ($n = 5$) from 2.5 to 3 dpf (mean ± SD; Student's *t* test; nonsignificant [ns] $P > 0.05$, $^{***}P < 0.001$). (*D*) Representative tail images of peripheral macrophages surrounding the injury sites 6 h post injury (hpi) in 3 dpf siblings, *mafba* mutants, *mafbb* mutants, and DMut in *Tg(mpeg1:DsRedx)* transgenic background. Macrophages are labeled in red color. (*E*) Quantification of peripheral macrophages surrounding the injury sites 6 h post injury in 3 dpf siblings ($n = 11$), *mafba* mutants ($n = 8$), *mafbb* mutants ($n = 10$), and DMut ($n = 15$) in *Tg(mpeg1:DsRedx)* transgenic background (mean ± SD; Student's *t* test; nonsignificant [ns] $P > 0.05$, $^*P < 0.05$).

As Mafba and Mafbb are transcription factors and act cell-autonomously, we reasoned that they likely regulated microglia colonization through modulating the expression of cell surface receptors capable of recognizing the chemoattractants released from apoptotic neurons (13, 14). Indeed, RNA-seq data analysis revealed that, among those known chemoattractant receptors (34) such as lysophosphatidylcholine (LPC), sphingosine-1-phosphate (S1P), nucleotides, fractalkine, and lysophosphatidylserine (lysoPS) (35–37), three nucleotide receptors (purinergic receptors *p2rx7*, *p2ry11*, and *p2ry12*) (38) and one lysoPS receptor (G protein–coupled receptor *gpr34a*) (39, 40), were highly expressed in siblings, *mafba* and *mafbb* single mutants but were largely abolished in DMut (Fig. 4*B*), suggesting that these receptors are downstream targets of Mafba and Mafbb. Notably, despite the absence of microglia markers, such as *apoeb* (29) and *ccl34b.1* (41), in DMut, the expression of transcription factors, such as *spi1a*, *spi1b*, and *irf8*, essential for macrophage development (42, 43), and other macrophage/myeloid signature genes, such as *coro1a* (44), *mpeg1.1* (45), *lcp1* (29), and *csf1ra* (29), are relatively normal (*SI Appendix*, Fig. S6 *A–C*), showing that the

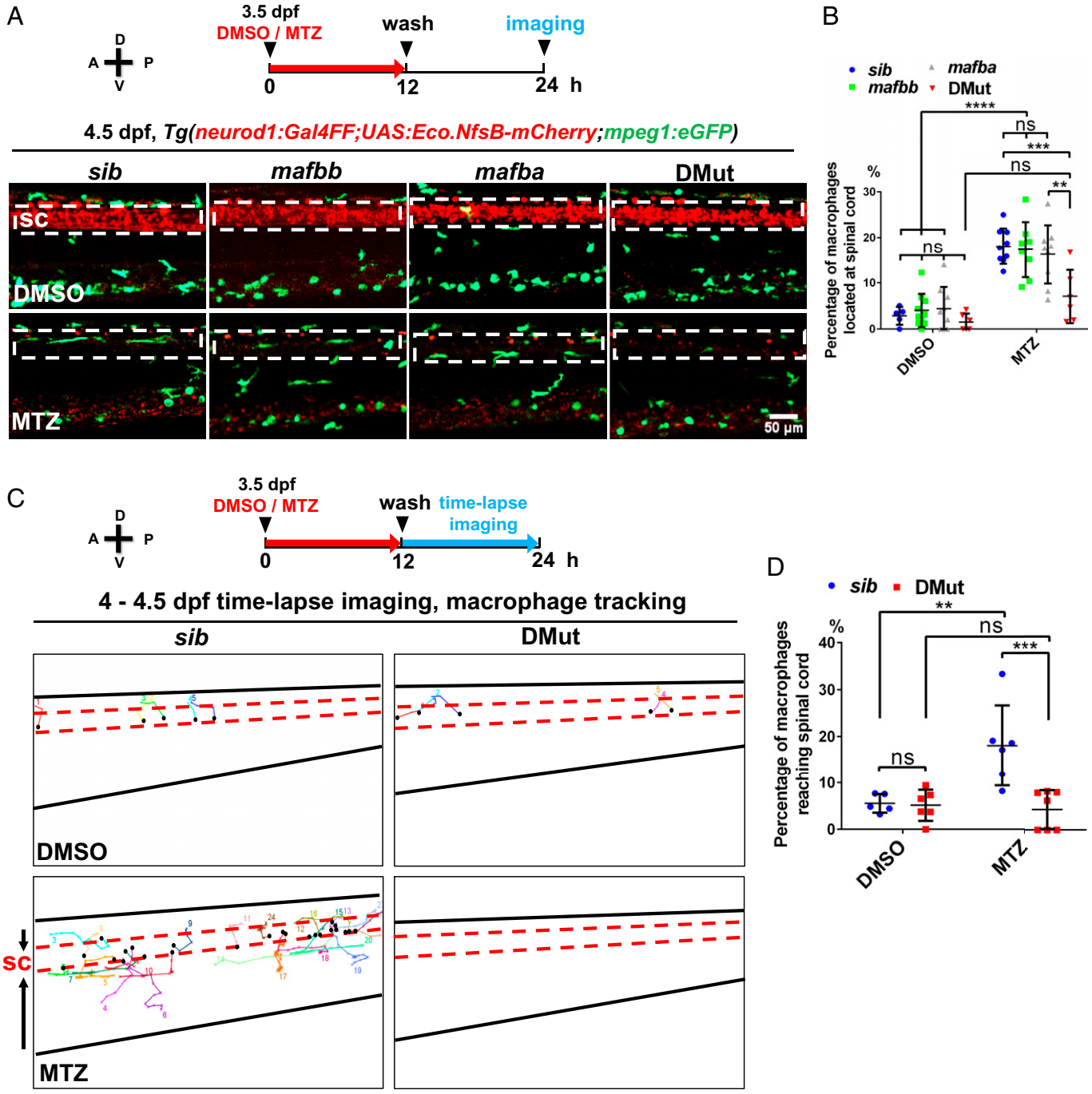

Fig. 3. Macrophages in DMut fail to respond to the induction of neuronal apoptosis. (*A*) *Upper Panel*: schematic diagram of the workflow of neuronal cell death induction and imaging. A, anterior; P, posterior; D, dorsal; V, ventral. *Lower Panel*: representative images of the trunk region of 4.5 dpf siblings, *mafba* mutants, *mafbb* mutants, and DMut in *Tg(neurod1:Gal4FF;UAS:Eco.NfsB-mCherry;mpeg1:eGFP)* triple-transgenic background. *Top* groups are DMSO-treated and *Bottom* groups are MTZ-treated. Red and green signals represent neurons and macrophages, respectively. White dashed lines indicate the spinal cord region. sc, spinal cord. (*B*) Percentage of macrophages around the spinal cord region to total macrophages in siblings (n = 5 for DMSO or 9 for MTZ), *mafba* mutants (n = 9 for DMSO or 9 for MTZ), *mafbb* mutants (n = 10 for DMSO or 8 for MTZ), and DMut (n = 6 for DMSO or 6 for MTZ) treated with DMSO or MTZ at 4.5 dpf (mean ± SD; two-way ANOVA; nonsignificant [ns] $P > 0.05$, $^{**}P < 0.01$, $^{***}P < 0.001$, $^{****}P < 0.0001$). (*C*) The mobilization trajectory (from 4 dpf to 4.5 dpf) of macrophages in the trunk of siblings and DMut in *Tg(neurod1:Gal4FF;UAS:Eco.NfsB-mCherry;mpeg1:eGFP)* triple-transgenic background after DMSO or MTZ treatment. The fish trunk and spinal cord region are indicated by black lines and red dashed lines, respectively. The numbers and black dots indicate start and end points of trajectories, respectively. (*D*) Percentage of macrophages reaching spinal cord to total macrophages during the imaging period (from 4 dpf to 4.5 dpf) in siblings (n = 5 for DMSO or 6 for MTZ) and DMut embryos (n = 6 for DMSO or 7 for MTZ) (mean ± SD; two-way ANOVA; non-significant [ns] $P > 0.05$, $^{**}P < 0.01$, $^{***}P < 0.001$.

development of macrophages in DMut is not broadly affected. Taken together, these data demonstrate that the down-regulation of chemotaxis receptors could be the main cause of microglial colonization defect in DMut.

Considering that the expression level of *gpr34a* is the highest among all these receptors in microglia and its expression is completely abolished in DMut (Fig. 4*B*), we reasoned that the down-regulation of *gpr34a* could be one of the major causes for the microglia defect in DMut. To support this speculation, we first validated the expression of *gpr34a* in microglia by RNA-scope single-molecule fluorescent in situ hybridization in siblings, *mafba* and *mafbb* single mutants, and DMut. Consistent

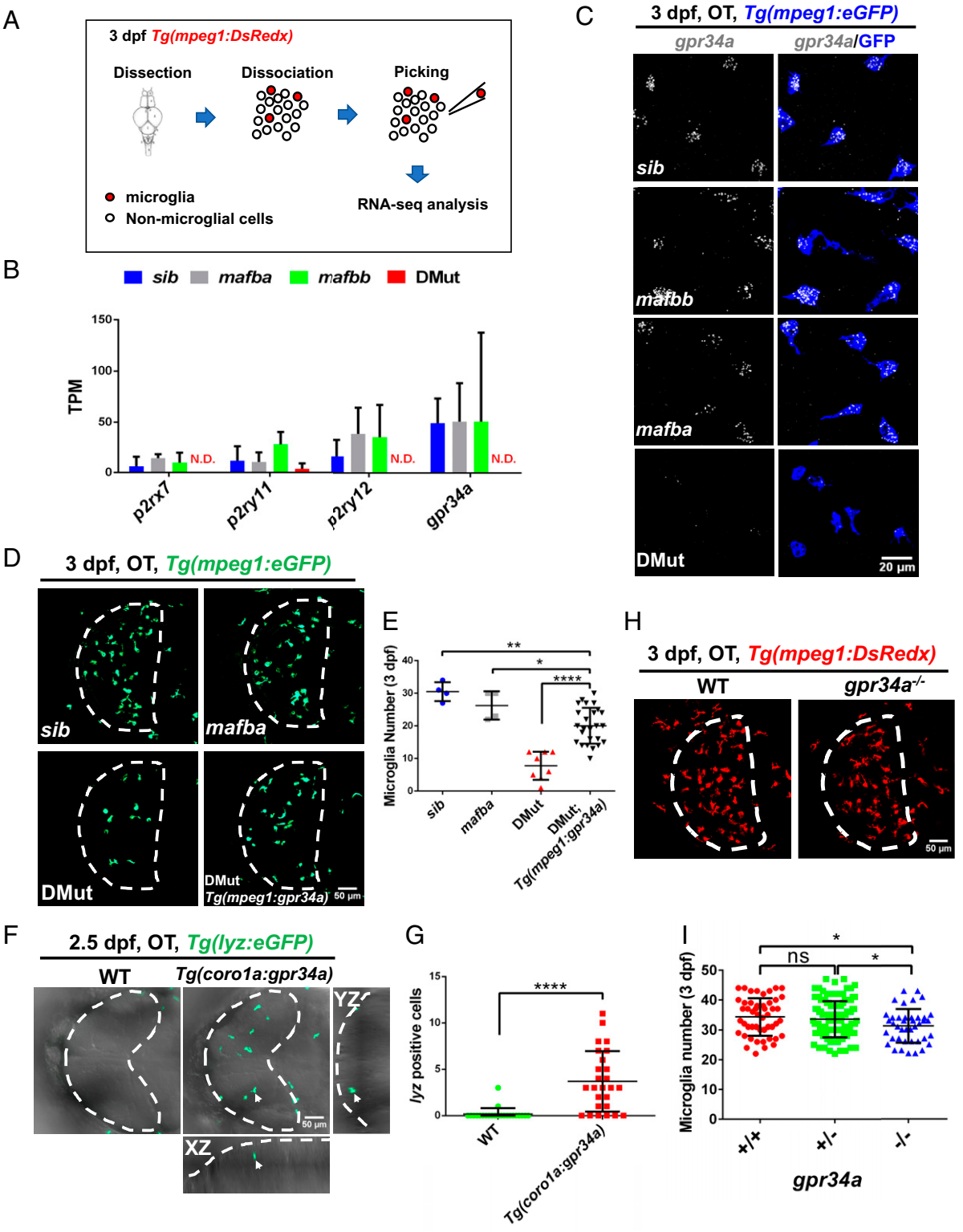

Fig. 4. Gpr34a is a downstream target of Mafba and Mafbb and promotes microglia colonization. (*A*) Workflow of microglia isolation from the brains of 3 dpf siblings, *mafba* mutants, *mafbb* mutants and DMut for transcriptomic analysis. (*B*) Expression level of *p2rx7*, *p2ry11*, *p2ry12*, and *gpr34a* in siblings, *mafba* mutants, *mafbb* mutants, and DMut embryos in RNA-seq data. $n = 3$ for each group. TPM, transcript per million. N.D., not detected. (*C*) Representative images of *gpr34a* RNAscope (gray) and anti-GFP antibody staining (blue) in the optic tectum (OT) of 3 dpf siblings, *mafba* mutants, *mafbb* mutants, and DMut in *Tg(mpeg1:eGFP)* transgenic background. (*D*) Representative images of microglia in the OT region in 3 dpf siblings, *mafba* mutants, DMut embryos, and DMut;*Tg(mpeg1:gpr34a)* transgenic embryos. Microglia are labeled in green color in *Tg(mpeg1:eGFP)* transgenic background. Dashed lines indicate the OT region. (*E*) Quantification of microglia number in the OT region in 3 dpf siblings ($n = 4$), *mafba* mutants ($n = 4$), DMut embryos ($n = 8$), and DMut;*Tg(mpeg1:gpr34a)* transgenic embryos ($n = 25$) in *Tg(mpeg1:eGFP)* transgenic background (mean ± SD; Student's *t* test; $^{*}P < 0.05$, $^{**}P < 0.01$, $^{****}P < 0.0001$). (*F*) Representative images of neutrophils in the OT region in 2.5 dpf wild-type (WT) and *Tg(coro1a:gpr34a)* transgenic embryos. Neutrophils are labeled in green color. Dashed lines indicate the OT region. White arrow indicates a neutrophil located in the OT. (*G*) Quantification of neutrophils in the OT region in 2.5 dpf WT ($n = 23$) and *Tg(coro1a:gpr34a)* transgenic embryos ($n = 26$) (mean ± SD; Student's *t* test; $^{****}P < 0.0001$). (*H*) Representative Images of microglia in the OT in 3 dpf WT and *gpr34a* mutants in *Tg(mpeg1: DsRedx)* transgenic background. Microglia are labeled in red color. Dashed lines indicate the OT region. (*I*) Quantification of microglia number in the OT in 3 dpf WT ($n = 49$), *gpr34a* heterozygous embryos ($n = 124$), and *gpr34a* mutants ($n = 41$) in *Tg(mpeg1: DsRedx)* transgenic background (mean ± SD; Student's *t* test; nonsignificant [ns] $P > 0.05$; $^{*}P < 0.05$).

with the RNA-seq data, results showed that *gpr34a* manifested robust expression in the microglia of siblings, *mafba* and *mafbb* single mutants, while its expression was largely absent in DMut (Fig. 4*C*). To directly address whether Gpr34a acts downstream of Mafba and Mafbb, we generated a *gpr34a* overexpression transgenic line *Tg(mpeg1:gpr34a)*, in which overexpression of *gpr34a* was under the control of the macrophage-specific *mpeg1* promoter (45) (*SI Appendix*, Fig. S7*A*), and tested whether reconstitution of *gpr34a* expression in microglia/macrophages was able to rescue the microglia phenotype in DMut. Indeed, microglia number was partially restored in *Tg(mpeg1:gpr34a)*;DMut transgenic mutants (Fig. 4 *D* and *E*). The rescue effect by *gpr34a* overexpression was not due to the increase of macrophages as the number of peripheral macrophages remained largely unchanged in *Tg(mpeg1:gpr34a)*;DMut fish (*SI Appendix*, Fig. S7*B*). To further prove that Gpr34a could indeed function as chemoattractant receptors, we ectopically overexpressed *gpr34a* in neutrophils by the myeloid-specific *coro1a* promoter (44) (*SI Appendix*, Fig. S7*C*), and as expected, ectopically overexpressing *gpr34a* was able to direct neutrophils to colonize the brain (Fig. 4 *F* and *G*). From these results, we conclude that *gpr34a* is a downstream target of Mafba and Mafbb, and the microglial colonization defect in DMut is attributed, at least in part, to the loss of *gpr34a* expression.

In parallel, we employed CRISPR-Cas9 system and generated a loss of function allele *gpr34a*$^{\Delta 755}$, which carries 760-bp deletion and 5-bp insertion in the coding region of *gpr34a* gene, resulting in the production of a truncated protein devoid of most transmembrane domains (*SI Appendix*, Fig. S8 *A* and *B*). Results showed that *gpr34a* mutants displayed a moderate, but statistically significant, reduction of *mpeg1*$^{+}$ microglia at 3 dpf (Fig. 4 *H* and *I*), suggesting that Gpr34a plays a role in mediating microglial colonization. However, the microglia phenotype in *gpr34a* mutants appeared to be much weaker than that in DMut (Fig. 1 *A* and *B*). We therefore reasoned that other chemotaxis receptors capable of sensing apoptotic neuron-secreted molecules may compensate the loss of Gpr34a function to mediate microglial colonization in *gpr34a* mutants (46). Indeed, real-time qPCR showed that the expression levels of several chemotaxis receptors, including lysoPS receptors (*gpr174* and *p2ry10*) (40), LPC receptors (*gpr132a* and *gpr132b*) (13), and purinergic receptors (*p2rx7*, *p2ry11*, and *p2ry12*) (38) which were expressed in the microglia in siblings, *mafba* and *mafbb* single mutants but largely absent in DMut (Fig. 4*B*), were largely unaffected or markedly increased in *gpr34a* mutants (*SI Appendix*, Fig. S8*C*). Notably, among these receptors, the purinergic receptor P2ry12 has been shown to mediate microglia chemotaxis through ADP/ATP in zebrafish and mice (47, 48). We therefore tested whether P2ry12 could act as a chemotaxis receptor to sense chemotactic signals from apoptotic neurons to direct cells into the developing zebrafish brain. Indeed, we showed that ectopically overexpressing *p2ry12* was able to recruit neutrophils into the brain in wild-type and DMut fish (*SI Appendix*, Fig. S9). These results indicate that the neuronal apoptosis-mediated microglial colonization is regulated by diversified chemotaxis receptors capable of sensing various chemoattractant signals released from the apoptotic neurons.

Peripheral Macrophages in DMut Fail to Respond to Lysophosphatidylserine. Having demonstrated that Gpr34a is one of the key chemotaxis receptors mediating microglial colonization of the optic tectum, we were next keen to identify the corresponding chemoattractant signals released from apoptotic neurons. In previous studies, transwell cell migration assays revealed that lysoPS, an apoptotic-cell-secreted signaling phospholipid (49), can stimulate cell chemotactic migration via GPR34 receptors (35–37). We therefore speculated that lysoPS could be a potent chemoattractant secreted by the apoptotic neurons to attract peripheral macrophages to colonize developing zebrafish brain. To support this hypothesis, we directly injected lysoPS or saline solution (phosphate-buffered saline [PBS]) into one side of the midbrain of 3 dpf *Tg(Xla.Tubb:bcl-2;mpeg1:DsRedx)* transgenic fish embryos (Fig. 5*A*), in which microglial colonization of the optic tectum is largely blocked due to the suppression of neuronal death (13). As shown in *SI Appendix*, Fig. S10, lysoPS injection recruited more than twofold increase of microglia in the midbrain compared to the PBS injection (*SI Appendix*, Fig. S10 *A* and *B*). This effect appeared to be direct and specific as lysoPS injection did not induce obvious neuronal apoptosis (*SI Appendix*, Fig. S10*C*). To confirm that lysoPS-induced microglial colonization was mediated through Gpr34a and this lysoPS-Gpr34a axis was perturbed in DMut, we injected lysoPS into one side of the midbrain of 3 dpf siblings, *mafba* single mutants, *mafbb* single mutants, and DMut under the *Tg(Xla.Tubb:bcl-2;mpeg1:DsRedx)* transgenic background. Results showed that, while peripheral macrophages responded robustly or moderately to lysoPS in siblings and single mutants, respectively, the peripheral macrophages in DMut barely responded to lysoPS (Fig. 5 *B* and *C*). Interestingly, peripheral macrophages in *gpr34a* mutants could still respond to lysoPS (*SI Appendix*, Fig. S10 *D* and *E*), suggesting the existence of the compensatory effect by other lysoPS receptors in *gpr34a* mutants (*SI Appendix*, Fig. S8*C*). Collectively, these data indicate that lysoPS released by apoptotic neurons is an essential guidance cue for peripheral macrophage colonization of the brain and the unresponsiveness of microglia/macrophages to lysoPS is one of the major causes for microglial colonization defect in DMut.

Discussion

In this study, by combining genetic analysis, in vivo time-lapse imaging, and transcriptomic analysis, we demonstrated that microglial colonization of zebrafish optic tectum is regulated by Mafba and Mafbb through modulating the lysoPS-Gpr34a signaling pathway.

An interesting observation is that Mafba and Mafbb are essential for the homing of macrophages from peripheral tissues to the CNS (Fig. 2 *B* and *C*) but dispensable for wound-induced and bacteria-induced migration of macrophages (Fig. 2 *D* and *E* and *SI Appendix*, Fig. S2 *C* and *D*). These results indicate that the unresponsiveness of microglial precursors/macrophages to brain-derived apoptotic signals is specifically controlled by Mafba and Mafbb. Given the fact that the pathogen-associated molecular patterns (PAMPs) and DAMPs released from pathogens or damaged cells are quite different from those of "find-me" signals released by apoptotic cells (34, 50), we speculate that Mafba and Mafbb specifically and directly regulate the expression of a group of receptors recognizing the find-me signals released from the apoptotic cells but not those recognizing PAMPs and DAMPs. This notion is supported by several lines of evidence. First, lysoPS receptor (*gpr34a*) and nucleotide receptors (*p2rx7*, *p2ry11*, and *p2ry12*) are largely abolished in DMut fish (Fig. 4*B*). Second, analysis of the promoter regions of mammalian *Gpr34* and three purinergic receptors *p2rx7*, *p2ry11*, and *p2ry12* in zebrafish and mammals revealed several potential and conserved half Maf recognition elements (half-MAREs) (*SI Appendix*, Fig. S11). Moreover, MafB chromatin immunoprecipitation sequencing

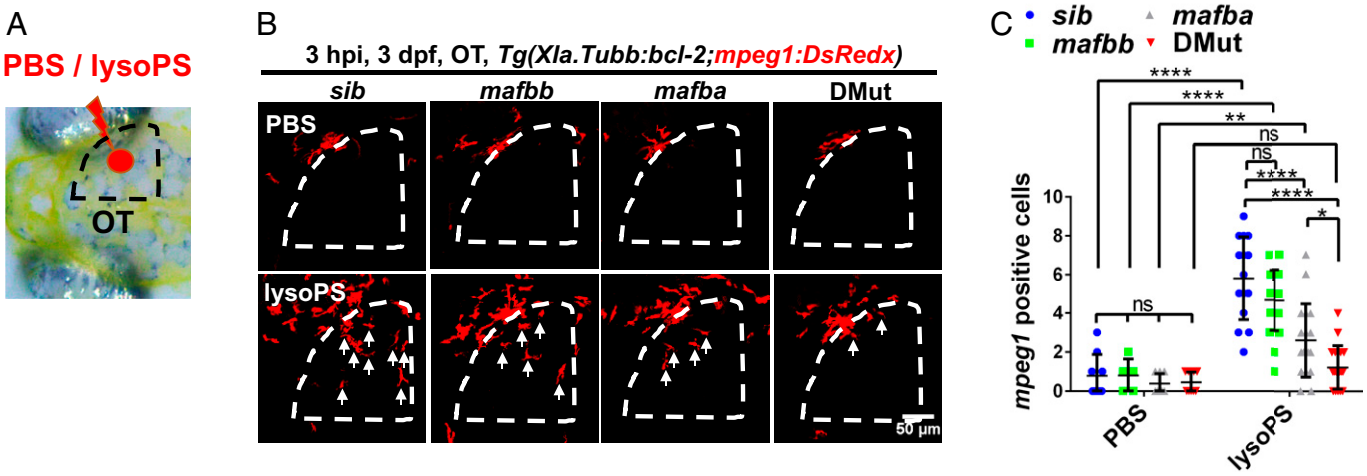

Fig. 5. Macrophages in DMut do not respond to lysoPS. (*A*) Schematic diagram indicates the PBS/lysoPS injection region. (*B*) Representative images of recruited macrophages in the optic tectum (OT) region in PBS/lysoPS-injected siblings, *mafba* mutants, *mafbb* mutants, and DMut embryos in *Tg(Xla.Tubb:bcl-2;mpeg1:DsRedx)* double-transgenic background. Macrophages are labeled in red color. Dashed lines indicate the optic tectum region. Arrows represent recruited macrophages in the OT. hpi, hours post injection. (*C*) Quantification of recruited macrophage number in the OT region in PBS/lysoPS-injected siblings (n = 9 for PBS or 15 for lysoPS), *mafba* mutants (n = 8 for PBS or 18 for lysoPS), *mafbb* mutants (n = 5 for PBS or 21 for lysoPS), and DMut embryos (n = 9 for PBS or 18 for lysoPS) in *Tg(Xla.Tubb:bcl-2;mpeg1:DsRedx)* double-transgenic background (mean ± SD; two-way ANOVA; nonsignificant [ns] $P > 0.05$, *$P < 0.05$, **$P < 0.01$, ****$P < 0.0001$).

(ChIP-seq) data from mouse bone marrow-derived macrophages showed that MafB ChIP-seq signals are enriched in the promoter regions of *Gpr34*, *P2rx7*, and *P2ry12* (*P2ry11* gene is absent in mice) (51) (*SI Appendix*, Fig. S11), indicating MafB directly regulates *Gpr34*, *P2rx7*, and *P2ry12* expression. We thus believe that *mafba* and *mafbb* may also directly regulate the expression of lysoPS receptor (*gpr34a*) and nucleotide receptors (*p2rx7*, *p2ry11*, and *p2ry12*). Intriguingly, one of adenosine receptors, adenosine A2b receptor (*adora2b*) which has been implicated in chemorepulsion (52) was also found to increase in DMut, although its expression level in macrophages/microglia appears to be less robust than that of those chemotaxis receptors (*SI Appendix*, Fig. S6*D*). Whether the alteration of the *adora2b* expression contributes to the microglia homing defect in DMut remains unclear. It will be of great interest to explore whether the mammalian MAFB has similar roles in the regulation of microglial colonization.

Our results showed that the loss of Gpr34a function has a moderate effect on microglial colonization in zebrafish, which is much weaker than that in DMut. One possible explanation is that the loss of Gpr34a function could be compensated by two other GPR34 orthologs, Gpr34b and Gpr34l which share 30–50% similarity with Gpr34a in protein sequence (*SI Appendix*, Fig. S12), possibly through the mutant mRNA decay pathway (53, 54). However, we found that *gpr34b* and *gpr34l* expression are undetectable in macrophages/microglia in both wild-type and *gpr34a* mutants (*SI Appendix*, Fig. S8*C*), suggesting that the mild microglial phenotype in *gpr34a* mutants is unlikely to be a result of the complementary effect of *gpr34b* and *gpr34l*. Interestingly, we found that the expression of *p2ry10*, another well-known lysoPS receptor (40), and a member of LPC receptors *gpr132a* (13) are markedly increased in *gpr34a*-deficient macrophages/microglia (*SI Appendix*, Fig. S8*C*), raising the possibility that the loss of Gpr34a function could be compensated by the up-regulation of *p2ry10* and *gpr132a*. Furthermore, purinergic receptors *p2rx7*, *p2ry11*, and *p2ry12*, which are believed to be able to mediate microglia chemotaxis in zebrafish and mice (14, 47, 48), are robustly expressed in *gpr34a* mutants (*SI Appendix*, Fig. S8*C*) but largely abolished in DMut (Fig. 4*B*), suggesting that the purinergic receptors may also compensate the loss of Gpr34a function. This notion is further supported by the findings that ectopically overexpressing *p2ry12* in neutrophils can trigger neutrophil infiltrating the brain in zebrafish (*SI Appendix*, Fig. S9). Further in-depth study will be needed to delineate the contributions of 'find-me' signals and their receptors to microglia colonization.

Another interesting but unaddressed question is why multiple find-me signals and their receptors are involved in neuronal apoptosis-mediated microglia colonization during early zebrafish development. It is well-known that in higher organisms including zebrafish, a substantial number of neurons undergo apoptosis during early neurogenesis (29, 55) and proper removal of these dying neurons appears to be critical for CNS development and homeostasis (56). Hence, utilization of multiple receptors capable of sensing a variety of signaling molecules released from apoptotic neurons will facilitate the colonization of the brain by peripheral macrophages, thereby protecting zebrafish from deleterious mutations that affect one or more signaling pathway(s). Alternatively, the amount of chemoattractants released from apoptotic neurons could be limited and are rapidly degraded in extracellular environment (57) so that these signals need to be quickly captured by peripheral macrophages/microglial precursors to recruit them to the brain. Finally, but not least, we also noticed that, in addition to functioning as chemoattractants, some of these apoptotic cells-derived signals also play an important role in the clearance of apoptotic cells, as evidenced by the findings showing that lysoPS secreted from apoptotic cells can enhance the clearance of apoptotic cells by macrophages (58, 59). The dual functions of these signals couple the recruitment of microglia with the phagocytosis to enhance the clearance of the apoptotic neurons.

Materials and Methods

Zebrafish. All zebrafish lines were maintained under standard protocols (60). AB wild-type, *Tg(mpeg1:eGFP)* (42), *Tg(mpeg1:loxP-DsRedx-loxP-GFP)* (13), *Tg(-2.8elavl3:eGFP)* (61), *Tg(Xla.Tubb:bcl-2)* (13), *Tg(neurod1:Gal4FF)* (31), *Tg(UAS:Eco.NfsB-mCherry)* (32), *Tg(lyz:eGFP)* (62), *Tg(mfap4:mafba-P2a-DsRedx)*^{hkz042Tg}, *Tg(mfap4:mafbb-P2a-DsRedx)*^{hkz043Tg}, *Tg(mpeg1:gpr34a-P2a-mCherry)*^{hkz044Tg}, *Tg(coro1a:gpr34a)*^{hkz045Tg}, *mafba*^{uq4bh} (28), *mafbb*^{hkz16}, and

gpr34a^{hkz17} were used in this study. All animal experiments were carried out under the approval from the Hong Kong University of Science and Technology's Animal Studies Committee.

Generation of Transgenic and Mutant Lines. The DsRedx gene was PCR-amplified using a pair of primers that contained a *P2a* self-cleaving peptide sequence. The *mfap4* promoter (30), coding sequences of *mafba* or *mafbb*, and *P2a-DsRedx* were cloned into pTol2 vector to generate *mfap4:mafba-P2a-DsRedx* and *mfap4:mafbb-P2a-DsRedx* plasmids. Similarly, the *mpeg1* promoter (45) coding sequences of *gpr34a* and *P2a-mCherry* were cloned into pTol2 vector to generate *mpeg1:gpr34a-P2a-mCherry* plasmid. The *coro1a* promoter (44) and coding sequence of *gpr34a*, *p2rx7*, *p2ry11*, and *p2ry12* were cloned into pTol2 vector to generate *coro1a:gpr34a*, *coro1a:p2rx7*, *coro1a:p2ry11*, and *coro1a:p2ry12* plasmids, respectively. The purified vectors (25 ng/μL) and mRNA of transposase (50 ng/μL) were injected into fertilized embryos at one cell stage (63). The injected embryos were raised to adult and outcrossed with WT for germline transmission screening. The *mafbb* mutants and *gpr34a* mutants were generated by CRISPR/Cas9 as previously reported (12). The primers used for gRNA synthesis and genotyping were listed in *SI Appendix*, Table S1.

Fluorescent In Situ Hybridization (FISH) and Immunofluorescent Antibody Staining. The antisense DIG-labeled RNA probes of *mafba*, *mafbb*, and *gpr34a* were generated in vitro. FISH was carried out as previously reported (64). In brief, embryos were firstly treated as previous description: fixation, dehydration, rehydration, permeabilization, and hybridization with the RNA probe. After that, embryos were incubated with 2% blocking reagent (11096176001, Roche) in MABT for 1 h at room temperature, then with Anti-Digoxigenin-POD (11207733910, Roche) (1:2,000 dilution in blocking buffer) at 4 °C overnight. After washing with MABT for several times, embryos were stained with TSA Plus Cyanine 3 System (NEL744001KT, Perkin-Elmer). After that, the embryos were incubated with goat anti-GFP (ab6658, Abcam) or rabbit anti-Lcp1 primary antibody (65) at 4 °C overnight, followed with incubation of Alexa Fluor 488-anti-goat (A11055, Thermo Fisher) or Alexa Fluor 488-anti-rabbit (A21206, Thermo Fisher) secondary antibody at 4 °C overnight, respectively.

Neutral Red (NR), Acridine Orange (AO), and Sudan Black B (SB) Staining. NR (N6264, Sigma), AO (A6014, Sigma) and SB staining (199664, Sigma) were performed as previously reported (66).

Time-Lapse Imaging, Cell Tracking Analysis, and 2D Speed Measurements. Time-lapse imaging was performed as previously reported (12, 13). For imaging microglia colonization of the optic tectum from 2.5 dpf to 3 dpf, a 20× objective was used on Zeiss LSM 980 and the system was set as 3-μm Z step size and around 40 planes in the Z-stack at an approximately 3.5-min interval for each embryo. For tracking the migration of peripheral macrophages after the induction of neuronal apoptosis from 4 dpf to 4.5 dpf, a 10× objective was used on Zeiss LSM 980, and the system was set as 14-μm Z step size and 14–16 planes in the Z-stack at an approximately 5- to 6-min interval for each embryo. The time-lapse imaging was processed with ImageJ software. The cell tracking and mean velocity of peripheral macrophages were analyzed by MTrackJ plugin on ImageJ software.

Cryosection and Immunostaining. Cryosection and immunostaining of 3 dpf embryos were performed as previously described (12).

Tail Amputation. Tail amputation was carried out as previous described (44) and tail regions were imaged 6 h post injury.

Bacterial Inoculation. *E. coli* (containing pDSK-GFP) were prepared as previously reported (67) and injected into brain ventricle of the embryos at 2.5 dpf.

Induction of Neuronal Apoptosis. 3.5-dpf *Tg(neurod1:Gal4FF;UAS:Eco.NfsB-mCherry)* embryos were soaked in egg water containing 0.2% DMSO with or without 10 mM Metronidazole (MTZ) (M1547, Sigma) for 12 h at 28.5 °C. After changing to fresh egg water, embryos were anesthetized in 0.01% tricaine (A5040, Sigma) and embedded in the 1% low melting agarose for time-lapse imaging or incubated for another 12 h for imaging.

Cell Isolation and RNA-Seq. The brains were dissected from 3-dpf embryos (around 10 embryos for each genotype) and resuspended in 1 mL PBS with 5% FBS (5% FBS/PBS). The brain tissues were then digested by 0.5% dispase (4942078001, Roche) in 5% FBS/PBS at 37 °C for 20 min, followed by centrifugation at 1,000 rpm for 5 min. The brain cells were washed with 0.0125 U DNaseI (D4527, Sigma) in 20% FBS/PBS once and then with 5% FBS/PBS. The suspension was filtered through 40-μm Cell Strainer (352340, BD Falcon) and transferred to 35-mm Petri-dishes. DsRedx-positive cells were manually picked with the micromanipulator system (NT-88-V3, Nikon) under Nikon inverted microscopy. The picked cells were washed with RNase-free PBS containing 2% BSA once and transferred to 4.4 μL lysis buffer (0.2% Triton X-100 solution) in a 200-μL RNase-free tube. Three tubes (three cells in one tube) were prepared for each genotype. The reverse transcription and whole-transcriptome amplification was conducted according to the Smart-seq2 protocol (68). The quality of amplified cDNA was analyzed by Agilent Fragment Analyzer System and a total of 12 samples were sent to Novogene Company for Illumina sequencing with an average depth of 6×10^6 raw reads per sample. Raw reads were first aligned to zebrafish reference genome GRCz11.94 using STAR aligner. Read counts per gene were calculated by FeatureCounts (Rsubread_2.6.1). TPM (transcript per million) per gene were then calculated in R studio software.

Analysis of ChIP-Seq Data. Two ChIP-seq data sets, WT MafB (GSM1964739) and WT mouse bone marrow-derived macrophages input DNA (GSM1964741) (51), were reanalyzed. The reads were mapped to mouse genome and results were visualized and analyzed by Integrative Genomics Viewer (IGV) software.

RNAscope Assay and Immunofluorescent Antibody Staining. RNAscope assay on whole zebrafish embryos was conducted according to the manufacturer's instructions (Advanced Cell Diagnostics [ACD]) with the RNAscope Multiplex Fluorescent Reagent Kit (323100, ACD). The *gpr34a* probe (ACD catalog number: 1046341-C2; accession number: NM_001007215.1; target region: 312–1,169; probe dilution: 1:50) was generated by ACD company. After RNAscope assay, the embryos were incubated with the blocking buffer (5% FBS in PBST) at room temperature for 1 h and then incubated with goat anti-GFP primary antibody (ab6658; Abcam) as well as sequentially Alexa Fluor 488-anti-goat secondary antibody (A11055; Thermo Fisher) at 4 °C overnight.

Single-Cell Dissociation, Fluorescent-Activated Cell Sorting (FACS), cDNA Preparation, and Real-Time qPCR. Single-cell dissociation, FACS, cDNA preparation, and real-time qPCR were conducted as previously reported (69). Briefly, 3 dpf *Tg(mpeg1:DsRedx)* embryos (100 embryos in each genotype) were pooled together and dissociated into single cells. Five hundred DsRedx-positive cells were sorted into 4.4 μL lysis buffer (0.2% Triton X-100 solution) in a 200-μL RNase-free tube (four tubes per genotype) by FACS for cDNA preparation and real-time qPCR. Primers for qPCR are listed in *SI Appendix*, Table S1.

LysoPS Injection. The embryos at 3 dpf were anesthetized 0.01% tricaine (A5040; Sigma) and embedded in 1% low-melting agarose. Under Nikon inverted microscopy, lysoPS (5 mM) (858143, Avanti) was injected into one side of the brain by FemtoJet 4i and TransferMan 4r. The injection system was set as 150 hpa and 0.2 s.

Quantification and Statistical Analysis. Statistical parameter including the exact value of *n* and statistical significance are presented in the figures and figure legends. All the statistical analysis was performed using GraphPad Prism version 6. Data were presented as mean ± SD (SD). For pairwise comparisons, unpaired Student's *t* tests were used to calculate the two-tailed *P* value. For multiple comparisons, two-way ANOVA multiple comparison tests followed by Tukey's multiple comparisons test, and Sidak's multiple comparisons test were conducted to determine the significance.

Data, Materials, and Software Availability. All study data are included in the article and/or *SI Appendix*.

ACKNOWLEDGMENTS. We thank Drs. Benjamin M. Hogan, Anming Meng, Hae-Chul Park, and Phil Crosier for sharing *mafba*^{uq4bh} mutants, *Tg(-2.8elavl3:eGFP)*, *Tg(UAS:Eco.NfsB-mCherry)*, and *Tg(lyz:eGFP)* transgenic lines, respectively. We also thank Drs. Shuting Wu, Tienan Wang, Wan Jin, and Weilin Guo for technical support. This work was supported by the Major Program of Shenzhen Bay

Laboratory (S201101002), by the National Key Research and Development Program of China (2018YFA0800200), by the Research Grants Council of the Hong Kong (16103718, N_HKUST621/17, 16103920, T13-605/18-W, T13-602/21-N, and AoE/M-09/12), and by the Innovation and Technology Commission of the Hong Kong Special Administrative Region (ITCPD/17-9).

Author affiliations: [a]Division of Life Science, State Key Laboratory of Molecular Neuroscience, Center of Systems Biology and Human Health, the Hong Kong University of Science and Technology, Clear Water Bay, Kowloon, Hong Kong 999077, China; [b]Greater Bay Biomedical Innocenter, Shenzhen Bay Laboratory, Shenzhen 518055, China; [c]Shenzhen Peking University–Hong Kong University of Science and Technology Medical Center, Shenzhen 518055, China; and [d]Division of Cell, Developmental and Integrative Biology, School of Medicine, South China University of Technology, Guangzhou 510006, China

1. N. Lannes, E. Eppler, S. Etemad, P. Yotovski, L. Filgueira, Microglia at center stage: A comprehensive review about the versatile and unique residential macrophages of the central nervous system. *Oncotarget* **8**, 114393–114413 (2017).
2. D. A. Galloway, A. E. M. Phillips, D. R. J. Owen, C. S. Moore, Phagocytosis in the brain: Homeostasis and disease. *Front. Immunol.* **10**, 790 (2019).
3. M. W. Salter, S. Beggs, Sublime microglia: Expanding roles for the guardians of the CNS. *Cell* **158**, 15–24 (2014).
4. L. Muzio, A. Viotti, G. Martino, Microglia in neuroinflammation and neurodegeneration: From understanding to therapy. *Front. Neurosci.* **15**, 742065 (2021).
5. H. J. Yoo, M. S. Kwon, Aged microglia in neurodegenerative diseases: Microglia lifespan and culture methods. *Front. Aging Neurosci.* **13**, 766267 (2022).
6. C. Schulz *et al.*, A lineage of myeloid cells independent of Myb and hematopoietic stem cells. *Science* **336**, 86–90 (2012).
7. F. Ginhoux *et al.*, Fate mapping analysis reveals that adult microglia derive from primitive macrophages. *Science* **330**, 841–845 (2010).
8. K. Kierdorf *et al.*, Microglia emerge from erythromyeloid precursors via Pu.1- and Irf8-dependent pathways. *Nat. Neurosci.* **16**, 273–280 (2013).
9. C. Stremmel *et al.*, Yolk sac macrophage progenitors traffic to the embryo during defined stages of development. *Nat. Commun.* **9**, 75 (2018).
10. B. Arnò *et al.*, Neural progenitor cells orchestrate microglia migration and positioning into the developing cortex. *Nat. Commun.* **5**, 5611 (2014).
11. M. Hoshiko, I. Arnoux, E. Avignone, N. Yamamoto, E. Audinat, Deficiency of the microglial receptor CX3CR1 impairs postnatal functional development of thalamocortical synapses in the barrel cortex. *J. Neurosci.* **32**, 15106–15111 (2012).
12. S. Wu *et al.*, Il34-Csf1r pathway regulates the migration and colonization of microglial precursors. *Dev. Cell* **46**, 552–563.e4 (2018).
13. J. Xu, T. Wang, Y. Wu, W. Jin, Z. Wen, Microglia colonization of developing zebrafish midbrain is promoted by apoptotic neuron and lysophosphatidylcholine. *Dev. Cell* **38**, 214–222 (2016).
14. A. M. Casano, M. Albert, F. Peri, Developmental apoptosis mediates entry and positioning of microglia in the zebrafish brain. *Cell Rep.* **16**, 897–906 (2016).
15. L. Jing, L. I. Zon, Zebrafish as a model for normal and malignant hematopoiesis. *Dis. Model. Mech.* **4**, 433–438 (2011).
16. D. L. Stachura, D. Traver, Cellular dissection of zebrafish hematopoiesis. *Methods Cell Biol.* **101**, 75–110 (2011).
17. M. Hamada, Y. Tsunakawa, H. Jeon, M. K. Yadav, S. Takahashi, Role of MafB in macrophages. *Exp. Anim.* **69**, 1–10 (2020).
18. L. M. Kelly, U. Englmeier, I. Lafon, M. H. Sieweke, T. Graf, MafB is an inducer of monocytic differentiation. *EMBO J.* **19**, 1987–1997 (2000).
19. Y. Bakri *et al.*, Balance of MafB and PU.1 specifies alternative macrophage or dendritic cell fate. *Blood* **105**, 2707–2716 (2005).
20. C. Gemelli *et al.*, Virally mediated MafB transduction induces the monocyte commitment of human CD34+ hematopoietic stem/progenitor cells. *Cell Death Differ.* **13**, 1686–1696 (2006).
21. Y. Han *et al.*, Zebrafish *mafbb* mutants display osteoclast over-activation and bone deformity resembling osteolysis in MCTO patients. *Biomolecules* **11**, 480 (2021).
22. K. Kim *et al.*, MafB negatively regulates RANKL-mediated osteoclast differentiation. *Blood* **109**, 3253–3259 (2007).
23. M. T. N. Tran *et al.*, MafB is a critical regulator of complement component C1q. *Nat. Commun.* **8**, 1700 (2017).
24. T. Shichita *et al.*, MAFB prevents excess inflammation after ischemic stroke by accelerating clearance of damage signals through MSR1. *Nat. Med.* **23**, 723–732 (2017).
25. M. Hamada *et al.*, MafB promotes atherosclerosis by inhibiting foam-cell apoptosis. *Nat. Commun.* **5**, 3147 (2014).
26. O. Matcovitch-Natan *et al.*, Microglia development follows a stepwise program to regulate brain homeostasis. *Science* **353**, aad8670 (2016).
27. B. Blanchi *et al.*, MafB deficiency causes defective respiratory rhythmogenesis and fatal central apnea at birth. *Nat. Neurosci.* **6**, 1091–1100 (2003).
28. K. Koltowska *et al.*, mafba is a downstream transcriptional effector of Vegfc signaling essential for embryonic lymphangiogenesis in zebrafish. *Genes Dev.* **29**, 1618–1630 (2015).
29. P. Herbomel, B. Thisse, C. Thisse, Zebrafish early macrophages colonize cephalic mesenchyme and developing brain, retina, and epidermis through a M-CSF receptor-dependent invasive process. *Dev. Biol.* **238**, 274–288 (2001).
30. E. M. Walton, M. R. Cronan, R. W. Beerman, D. M. Tobin, The macrophage-specific promoter mfap4 allows live, long-term analysis of macrophage behavior during mycobacterial infection in zebrafish. *PLoS One* **10**, e0138949 (2015).
31. S. Lai *et al.*, Chemical screening reveals Ronidazole is a superior pro-drug to Metronidazole for nitroreductase-induced cell ablation system in zebrafish larvae. *J. Genet. Genomics* **48**, 1081–1090 (2021).
32. A. Y. Chung *et al.*, Generation of demyelination models by targeted ablation of oligodendrocytes in the zebrafish CNS. *Mol. Cells* **36**, 82–87 (2013).
33. S. Curado, D. Y. Stainier, R. M. Anderson, Nitroreductase-mediated cell/tissue ablation in zebrafish: A spatially and temporally controlled ablation method with applications in developmental and regeneration studies. *Nat. Protoc.* **3**, 948–954 (2008).
34. C. B. Medina, K. S. Ravichandran, Do not let death do us part: 'find-me' signals in communication between dying cells and the phagocytes. *Cell Death Differ.* **23**, 979–989 (2016).
35. Y. Iida *et al.*, Lysophosphatidylserine stimulates chemotactic migration of colorectal cancer cells through GPR34 and PI3K/Akt pathway. *Anticancer Res.* **34**, 5465–5472 (2014).
36. K. S. Park *et al.*, Lysophosphatidylserine stimulates L2071 mouse fibroblast chemotactic migration via a process involving pertussis toxin-sensitive trimeric G-proteins. *Mol. Pharmacol.* **69**, 1066–1073 (2006).
37. S. Y. Lee *et al.*, Lysophosphatidylserine stimulates chemotactic migration in U87 human glioma cells. *Biochem. Biophys. Res. Commun.* **374**, 147–151 (2008).
38. G. Burnstock, Purine and purinergic receptors. *Brain Neurosci. Adv.* **2**, 2398212818817494 (2018).
39. T. Sugo *et al.*, Identification of a lysophosphatidylserine receptor on mast cells. *Biochem. Biophys. Res. Commun.* **341**, 1078–1087 (2006).
40. A. Inoue *et al.*, TGFα shedding assay: An accurate and versatile method for detecting GPCR activation. *Nat. Methods* **9**, 1021–1029 (2012).
41. S. Wu *et al.*, Two phenotypically and functionally distinct microglial populations in adult zebrafish. *Sci. Adv.* **6**, eabd1160 (2020).
42. T. Yu *et al.*, Distinct regulatory networks control the development of macrophages of different origins in zebrafish. *Blood* **129**, 509–519 (2017).
43. L. Li, H. Jin, J. Xu, Y. Shi, Z. Wen, Irf8 regulates macrophage versus neutrophil fate during zebrafish primitive myelopoiesis. *Blood* **117**, 1359–1369 (2011).
44. L. Li, B. Yan, Y. Q. Shi, W. Q. Zhang, Z. L. Wen, Live imaging reveals differing roles of macrophages and neutrophils during zebrafish tail fin regeneration. *J. Biol. Chem.* **287**, 25353–25360 (2012).
45. F. Ellett, L. Pase, J. W. Hayman, A. Andrianopoulos, G. J. Lieschke, mpeg1 promoter transgenes direct macrophage-lineage expression in zebrafish. *Blood* **117**, e49–e56 (2011).
46. J. Peng, Gene redundancy and gene compensation: An updated view. *J. Genet. Genomics* **46**, 329–333 (2019).
47. D. Sieger, C. Moritz, T. Ziegenhals, S. Prykhozhij, F. Peri, Long-range Ca^{2+} waves transmit brain-damage signals to microglia. *Dev. Cell* **22**, 1138–1148 (2012).
48. S. E. Haynes *et al.*, The P2Y12 receptor regulates microglial activation by extracellular nucleotides. *Nat. Neurosci.* **9**, 1512–1519 (2006).
49. S. C. Frasch, D. L. Bratton, Emerging roles for lysophosphatidylserine in resolution of inflammation. *Prog. Lipid Res.* **51**, 199–207 (2012).
50. D. Tang, R. Kang, C. B. Coyne, H. J. Zeh, M. T. Lotze, PAMPs and DAMPs: Signal 0s that spur autophagy and immunity. *Immunol. Rev.* **249**, 158–175 (2012).
51. E. L. Soucie *et al.*, Lineage-specific enhancers activate self-renewal genes in macrophages and embryonic stem cells. *Science* **351**, aad5510 (2016).
52. R. Corriden, P. A. Insel, New insights regarding the regulation of chemotaxis by nucleotides, adenosine, and their receptors. *Purinergic Signal.* **8**, 587–598 (2012).
53. Z. Ma *et al.*, PTC-bearing mRNA elicits a genetic compensation response via Upf3a and COMPASS components. *Nature* **568**, 259–263 (2019).
54. M. A. El-Brolosy *et al.*, Genetic compensation triggered by mutant mRNA degradation. *Nature* **568**, 193–197 (2019).
55. F. Peri, C. Nüsslein-Volhard, Live imaging of neuronal degradation by microglia reveals a role for v0-ATPase a1 in phagosomal fusion in vivo. *Cell* **133**, 916–927 (2008).
56. M. Han *et al.*, Physiological roles of apoptotic cell clearance: Beyond immune functions. *Life (Basel)* **11**, 1141 (2021).
57. K. S. Ravichandran, Find-me and eat-me signals in apoptotic cell clearance: Progress and conundrums. *J. Exp. Med.* **207**, 1807–1817 (2010).
58. S. C. Frasch *et al.*, NADPH oxidase-dependent generation of lysophosphatidylserine enhances clearance of activated and dying neutrophils via G2A. *J. Biol. Chem.* **283**, 33736–33749 (2008).
59. S. C. Frasch *et al.*, Signaling via macrophage G2A enhances efferocytosis of dying neutrophils by augmentation of Rac activity. *J. Biol. Chem.* **286**, 12108–12122 (2011).
60. M. Westerfield, *The Zebrafish Book: A Guide for the Laboratory Use of Zebrafish (Danio Rerio)* (University of Oregon Press, 2000).
61. C. Zhao, X. He, C. Tian, A. Meng, Two GC-rich boxes in huC promoter play distinct roles in controlling its neuronal specific expression in zebrafish embryos. *Biochem. Biophys. Res. Commun.* **342**, 214–220 (2006).
62. C. Hall, M. V. Flores, T. Storm, K. Crosier, P. Crosier, The zebrafish lysozyme C promoter drives myeloid-specific expression in transgenic fish. *BMC Dev. Biol.* **7**, 42 (2007).
63. K. Kawakami, A. Shima, N. Kawakami, Identification of a functional transposase of the Tol2 element, an Ac-like element from the Japanese medaka fish, and its transposition in the zebrafish germ lineage. *Proc. Natl. Acad. Sci. U.S.A.* **97**, 11403–11408 (2000).
64. C. X. Zhang, F. Liu, [A brief protocol for high-resolution whole mount in situ hybridization in zebrafish]. *Yi Chuan* **35**, 522–528 (2013).
65. H. Jin *et al.*, Definitive hematopoietic stem/progenitor cells manifest distinct differentiation output in the zebrafish VDA and PBI. *Development* **136**, 647–654 (2009).
66. T. Wang *et al.*, Nlrc3-like is required for microglia maintenance in zebrafish. *J. Genet. Genomics* **46**, 291–299 (2019).
67. Y. Zeng *et al.*, In Vivo nonlinear optical imaging of immune responses: Tissue injury and infection. *Biophys. J.* **107**, 2436–2443 (2014).
68. S. Picelli *et al.*, Full-length RNA-seq from single cells using Smart-seq2. *Nat. Protoc.* **9**, 171–181 (2014).
69. Y. Tian *et al.*, The first wave of T lymphopoiesis in zebrafish arises from aorta endothelium independent of hematopoietic stem cells. *J. Exp. Med.* **214**, 3347–3360 (2017).